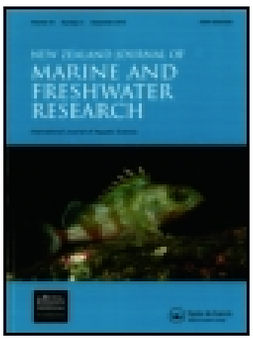

New Zealand Journal of Marine and Freshwater Research

ISSN: 0028-8330 (Print) 1175-8805 (Online) Journal homepage: http://www.tandfonline.com/loi/tnzm20

Wind-driven upwelling and surface chlorophyll blooms in Greater Cook Strait

Stephen M. Chiswell, John R. Zeldis, Mark G. Hadfield & Matthew H. Pinkerton

To cite this article: Stephen M. Chiswell, John R. Zeldis, Mark G. Hadfield & Matthew H. Pinkerton (2016): Wind-driven upwelling and surface chlorophyll blooms in Greater Cook Strait, New Zealand Journal of Marine and Freshwater Research, DOI: 10.1080/00288330.2016.1260606

To link to this article: http://dx.doi.org/10.1080/00288330.2016.1260606

Published online: 01 Dec 2016.

NEW ZEALAND JOURNAL OF MARINE AND FRESHWATER RESEARCH, 2016
http://dx.doi.org/10.1080/00288330.2016.1260606

Taylor & Francis
Taylor & Francis Group

RESEARCH ARTICLE

Wind-driven upwelling and surface chlorophyll blooms in Greater Cook Strait

Stephen M. Chiswell, John R. Zeldis, Mark G. Hadfield and Matthew H. Pinkerton

National Institute of Water and Atmospheric Research, Wellington, New Zealand

ABSTRACT

We present the results of a combined observational and numerical study to investigate cool plumes of nutrient-rich upwelled water that emanate near the Kahurangi Shoals and extend into Greater Cook Strait. Surface temperature and chlorophyll are mapped using satellite observations to produce surface climatologies, to validate a numerical simulation and to show the utility of using spatial temperature differences as a measure of upwelling. We find upwelling near the Kahurangi Shoals is strongly wind-driven in the weather band. Upwelling occurs at all times of the year, but its surface signature is only visible in summer months. The upwelled nutrient-rich water supports increased primary production compared to surrounding waters, particularly in summer when the water column is more stratified and surrounding surface waters are presumably nutrient depleted.

ARTICLE HISTORY
Received 21 July 2016
Accepted 5 November 2016

KEYWORDS
Upwelling; primary production; New Zealand; satellite observations; numerical simulation

Introduction

Cool plumes of nutrient-rich upwelled water have long been known to be generated within the Westland Current near the Kahurangi Shoals on the west coast of the South Island (Figure 1). These cool plumes are then carried by the d'Urville Current into Greater Cook Strait (GCS) and then into Cook Strait itself (Garner 1954; Stanton 1971). They carry enhanced nitrate levels (Foster & Battaerd 1985) and can support substantial primary production. Bradford and Chapman (1988) noted that concentrations of sea surface chlorophyll within the plumes can be four to six times greater than the background levels, although they noted that the highest surface chlorophyll is not necessarily coincident with the core of the plumes.

This biomass supports a food web leading to a squid-fishing industry in the region during the latter part of the twentieth century (Bowman et al. 1983). More recently, Torres (2013) suggested that the region is a blue whale foraging ground where whales feed on the euphausiid *Nyctiphanes australis* that concentrate in response to the enhanced primary production.

Shirtcliffe et al. (1990) reviewed early work in the region and stated that the first documentation of upwelling in the region was from commercial ships (Garner 1954), and that

CONTACT Stephen M. Chiswell s.chiswell@niwa.cri.nz

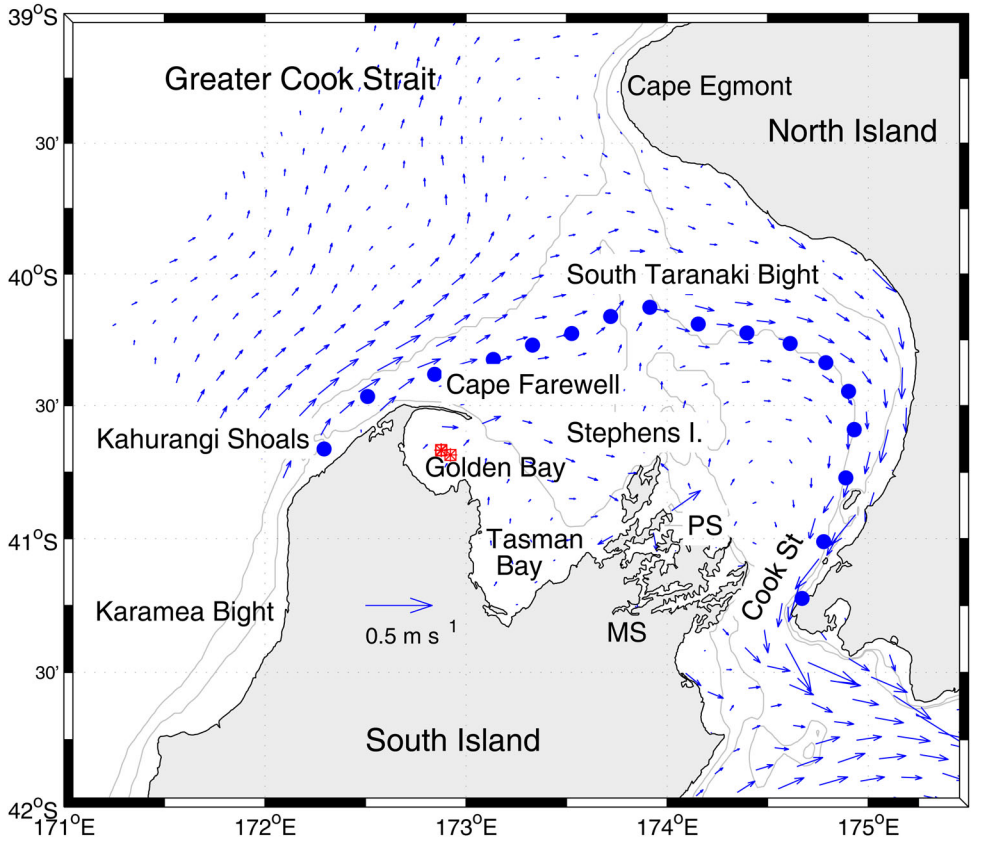

Figure 1. Locality map of GCS. Contours are 50 m and 100 m isobaths. Vectors are mean surface currents from the ROMS simulation (see text) plotted at one-third of the model resolution. The sequence of blue dots shows the daily locations of a numerical surface drifter released over the Kahurangi Shoals in this mean current. The red squares show the locations of the Golden Bay mooring, maintained from July 2010 until July 2011. MS = Marlborough Sounds, PS = Pelorus Sound.

the first detailed study of the area was by Stanton (1971) who showed upwelling was present during a survey of the region in March 1969, with coldest sea surface temperature found just north of the Kahurangi Shoals. Subsequently, Heath and Gilmour (1987) deployed a current meter off the Kahurangi Shoals for a month in mid-winter 1983 and concluded that daily mean along-shore currents are strongly correlated with the local along-shore wind – accounting for about 70% of the variance. Shirtcliffe et al. (1990) noted that 13 oceanographic cruises were made to the region before 1984, and that upwelling was observed in about half the cruises.

In their own work, Shirtcliffe et al. (1990), based on one week of observations in summer 1984, suggested the upwelling depends on the existence of the Westland Current, and is intensified by an on-shore (westerly) wind. They presented a model of the upwelling where this on-shore wind induces a fall in sea level near Cape Farewell. The resulting sea surface slope accelerates deep water over the bathymetric rise inshore of the Kahurangi Shoals. A hydraulic response of the thermocline coupled with coastal convergence of the bottom Ekman flow produces the upwelling.

Thus a picture emerges of intermittent upwelling along the northwest coast of the South Island between the north end of the Karamea Bight and Cape Farewell. The nutrient-rich upwelled water is brought into Cook Strait by the d'Urville Current. As it advects, this nutrient-rich water allows for primary production of phytoplankton long enough to sustain secondary production (Bradford & Chapman 1988), although the zooplankton species composition suggests that there is a mix of inshore water and upwelled waters within the plumes (Foster & Battaerd 1985). The plumes continue into Cook Strait, tending to flow along the eastern side of the strait (Stevens 2014). There may also be localised upwelling in the western side of Cook Strait, which also impacts the food web. Zeldis et al. (2013) showed that in summer, waters with an upwelling signature of cool surface temperature at the entrance of Pelorus Sound occurred under conditions of westerly wind stress at Farewell Spit, and that these upwelled waters carried elevated nitrate concentrations. These conditions correlated in turn with elevated seston (suspended particulate matter) concentrations within the Sound.

However, while these studies suggest that upwelling is dynamically favoured under westerly conditions, the mechanics of the upwelling in the region are not completely understood since this picture is based on relatively few cruises and limited direct observations. As Shirtcliffe et al. (1990) noted, the upwelling is not present in about half the observations, and most direct studies have been for periods of one to several weeks at the most (e.g. Heath & Gilmour 1987; Shirtcliffe et al. 1990). It seems likely that the upwelling is driven by south-westerly or westerly winds, although the roles of the Westland Current and any tidal mixing in both the upwelling process and supply of nutrients into the South Taranaki Bight are unknown. Both the frequency and duration of the upwelling events are not well known, nor is the impact of easterly or north easterly winds on surface temperature or surface chlorophyll.

The aims of this work are to understand more about the physical processes driving the upwelling, the frequency of upwelling and the relationship between surface temperature and surface chlorophyll. To address these aims we use a combined observational and numerical study to investigate the temporal and spatial nature of the upwelling and the plume. The observations include a short-term mooring in Golden Bay and 11 years of Moderate Resolution Imaging Spectroradiometer (MODIS, Esaias et al. 1998) satellite observations. The numerical simulation is a 7-year Regional Ocean Modeling System (ROMS) hindcast of the region.

One focus of this paper is to determine the relationships between surface temperature, upwelling and wind in the ROMS simulation, under the premise that the simulation correctly models the real world. However, before these relationships are investigated, one needs to evaluate the simulation. Thus the first sections of the Results are devoted to evaluating the simulation. With few current meter observations, this evaluation is based on how well the simulation reproduces satellite-derived surface temperature climatologies and satellite-derived indices of upwelling. Once the simulation has been evaluated, the last two sections of the Results consider the upwelling and its forcing in the simulation.

We also use the satellite data to derive climatologies of surface chlorophyll and the relationship between surface chlorophyll and surface temperature. Thus this paper serves both as a climatological description of the region and a description of the upwelling. More detailed analyses of the upwelling are reserved for later work.

Data and methods

For our purposes we consider GCS to cover the region shown in Figure 1, extending from Cook Strait proper in the south east to an imaginary line drawn between Cape Egmont and the Kahurangi Shoals. GCS encompasses the South Taranaki Bight, Tasman and Golden Bays, and the Marlborough Sounds.

The Kahurangi Shoals are situated on the west coast of the South Island, south west of Cape Farewell, and rise to just below sea level.

Golden bay mooring

An instrumented mooring was maintained in Golden Bay from July 2010 until July 2011. The mooring was deployed at 40°40.0′S, 172°52.7′E but halfway through the deployment was moved to 40°41.1′S, 172°55.4′E (see Figure 1). Both locations are in 30 m of water depth.

Instruments on the mooring included an Aanderaa RCM 9 current meter at 6 m below the surface, and an Ecotriplet (Wetlabs Inc., Oregon) and thermistor at 8 m below surface. The Ecotriplet sensors comprised two fluorometers (for chlorophyll-a and coloured dissolved organic matter) and a 532 nm backscatter sensor. Chlorophyll-a concentration was estimated by scaling fluorescence (excitation 470 nm, emission 695 nm) with no correction for photochemical quenching.

Near-surface (c. 8 m) temperature was returned from the mooring for the full deployment, but near-surface chlorophyll was returned only from July 2010 to March 2011.

MODIS Aqua satellite measurements of surface temperature and chlorophyll

Data from the MODIS (Esaias et al. 1998) flown on NASA's Aqua spacecraft were used to provide estimates of both surface temperature and surface chlorophyll. Level 1A (top of atmosphere, calibrated) MODIS Aqua data were acquired from the Ocean Biology Processing Group at NASA (pre-2007) and generated from locally received Level 0 data (post-2007), for GCS area.

Satellite data covered the period 1 January 2003 to 31 December 2013. Atmospheric correction was carried out using algorithms as implemented in the NASA ocean colour processing software SeaDAS v7.2 (e.g. Wang & Shi 2007). Both 'Case 1' (SeaDAS default band-ratio algorithm) and the 'Case 2' Quasi-Analytical Algorithm (QAA update v5, Lee et al. 2002, 2009) were used to estimate surface chlorophyll-a concentration, the latter using chlorophyll-specific absorption (Bricaud et al. 1995). The optical properties of water depend on the input of coloured material from rivers (which bring algae and suspended sediments into the coastal areas), resuspension of material from the seabed, and the populations of phytoplankton. The Case 1 product will overestimate surface chlorophyll where suspended sediment is present. A comparison of the Case 1 and 2 products (not shown) indicates that high suspended sediment waters are generally confined close to the shore and that the Case 1 product agreed better with mooring measurements. Hence the Case 1 product was used for surface chlorophyll. The MODIS Aqua daytime surface temperature product (MOD28, Walton et al. 1998) was used for surface temperature.

All satellite data products were produced at nominal 500 m resolution. Spatial and temporal composites of these products were created for this analysis. First, the 500-m data were spatially composited into 0.05° (c. 6 km) latitude by longitude bins, by selecting the median value. These spatial composites were then temporally composited into 5-day bins. Finally, any gaps in the time series were linearly filled to provide a gap-free data set for analysis.

ROMS simulation

The model code was the ROMS, which is a free-surface oceanic model that uses the hydrostatic and Boussinesq approximations to solve the three-dimensional Reynolds-averaged Navier-Stokes equations on an Arakawa C grid with a terrain-following vertical coordinate (Wilkin et al. 2005). The grid covered GCS at a uniform horizontal resolution of 2 km with 20 layers in the vertical dimension.

Lateral boundary data (velocity, temperature, salinity and sea surface height) were taken from daily snapshots of the HYCOM GLBa08 global analysis and forecast system. The model used nudged radiative boundary conditions (Marchesiello et al. 2001). Model temperature and velocity in the interior were also nudged towards the HYCOM daily data in a 15-cell-wide zone adjacent to each boundary, and at depth throughout the domain. The depth-dependent nudging rate was zero above 200 m and increased to $(20\ \mathrm{d})^{-1}$ at 800 m depth and below. The intention was to constrain the deep-ocean conditions with the HYCOM outer model but to allow the upper ocean to evolve freely.

Surface stresses were calculated from 3-hourly winds from the New Zealand Limited Area Model 12 km atmospheric analysis (see the next section). The standard formula relating wind speed to surface stress involves a wind-speed-dependent drag coefficient. For the present work this was calculated by the method of Smith (1988); however a comparison of preliminary model results with velocity measurements in Cook Strait narrows indicated that wind-driven variability in the model was too low. The drag coefficient was therefore multiplied by 1.2 to optimise agreement. A similar adjustment has been found to be necessary in previous modelling exercises around New Zealand by us and others (e.g. P. McComb pers. comm.).

Heat and moisture fluxes through the sea surface were calculated using 6-hourly average data from the National Centers for Environment Prediction (NCEP) reanalysis global atmospheric analysis system (Kalnay et al. 1996). The heat flux calculation included a correction term that causes the model sea surface temperature to be nudged towards a coarse-resolution surface temperature product, the NOAA Optimum Interpolation 1/4° daily surface temperature dataset (Reynolds et al. 2007). The heat flux correction was proportional to the difference between model SST and the NOAA product. The coefficient in this correction was 47 $\mathrm{W\ m^{-2}\ K^{-1}}$, which is sufficient to cause a 30 m thick surface mixed layer to relax towards the observed surface temperature with a e-folding time scale of 30 days. This prevents the modelled surface temperature from departing too far from reality due to any biases in the surface fluxes, but has a little effect on weather band variability.

The simulation was run from late 2007 to the end of 2014. Daily mean output was stored for analysis at full model resolution. These were then subsampled to the MODIS composite grid (c. 4 km zonal and 5 km meridional resolution).

Mean velocities were computed over the model years 2008 to 2013 and then used to simulate the trajectory of a surface drifter deployed at the Kahurangi Shoals, using conventional Runge-Kutta 4th-order advection routines. The daily locations of this drifter (e.g. Figure 1) give a visual indication of the centre of the plume.

New Zealand Limited Area Model (NZLAM) for winds

Hindcast winds were derived from the NZLAM. NZLAM is a local National Institute of Water and Atmospheric Research (NIWA) implementation of the United Kingdom Meteorological Office's Unified Model (Walters et al. 2014) at a horizontal resolution of 12 km. NZLAM is a non-hydrostatic, fully compressible, deep atmosphere formulation using a terrain-following height-based coordinate. NZLAM assimilates local data, including standard meteorological observations from land and ocean stations and satellite observations of atmospheric radiances, ocean winds using a 3DVAR+FGAT assimilation scheme (Lorenc et al. 2000). NZLAM hindcast 10 m winds were obtained on a c. 0.1° grid (Trevor Carey-Smith, unpublished data).

Results

Comparison of mooring and satellite data

Figure 2 shows near-surface temperature and chlorophyll from the Golden Bay mooring, along with 5-day composite surface temperature and surface chlorophyll from MODIS for the mooring location. Mooring data have been smoothed to match the 5-day compositing of the satellite data.

Near-surface temperature from the mooring, T_{moor}, spanned nearly an entire year, and satellite-derived sea surface temperature, T_{sat}, well match T_{moor}, with a mean temperature difference ($T_{sat} - T_{moor}$) of +0.12°C, and standard deviation (s.d.) of 0.6°C. The mean temperature is higher, and perturbations are greater, for the satellite product than for the mooring value. This likely reflects both the 8 m depth of the mooring thermistor and the spatial compositing of the satellite data.

The mooring fluorometer failed in March 2001. The resulting 9 months of inter-comparison data fail to capture the full annual cycle in chlorophyll, thus making evaluation of the satellite time series, C_{sat}, more difficult. However, the mooring signal, C_{moor}, has a 9-month decreasing trend that is well matched by a similar trend in C_{sat}. Also events each lasting 2–3 weeks (e.g. in July, August and December 2010) seen in C_{moor} are largely captured in C_{sat}. The chlorophyll difference ($C_{sat} - C_{moor}$) has a mean of +0.035 mg m^{-3} and s.d. of 1.7 mg m^{-3}.

Sea surface temperature climatology

Figure 3 shows the mean temperature averaged over the common time period (2008–2013) for both the satellite- and simulation-derived surface temperature, along with the difference between these means. Also shown are the mean wind fields from NZLAM for 2007–2012. The core of the plume is illustrated by daily locations of a particle released over the Kahurangi Shoals in the ROMS mean velocity field.

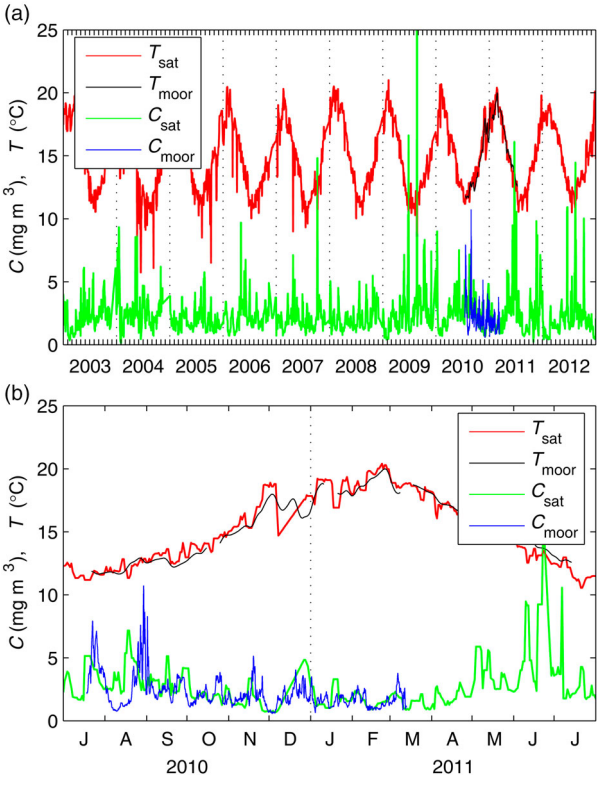

Figure 2. Comparison of MODIS satellite-derived surface temperature and chlorophyll with values from the mooring in Golden Bay (see Figure 1). (a) Sea surface temperature (T_{moor}) and sea surface chlorophyll (C_{moor}) from the Golden Bay mooring superimposed on sea surface temperature (T_{sat}) and sea surface chlorophyll (C_{sat}) from satellite measurements; (b) As in (a), but with expanded scale.

Mean surface temperature from the satellite observations, $\bar{T}_{sat}$, shows a plume of cool water extending from the Kahurangi Shoals past Farewell Spit and into GCS. The mean surface temperature over the Kahurangi Shoals is c. 14°C, and $\bar{T}_{sat}$ increases as one progresses along the core of the plume, eventually exceeding 15°C. A second region of cooler $\bar{T}_{sat}$ extending north from Cook Strait into GCS coincides with a region of weak cyclonic mean currents in the ROMS simulation (see Figure 1), and may reflect intense vertical mixing in Cook Strait driven by winds and or tides (Stevens 2014). The coolest $\bar{T}_{sat}$ in the region is less than 14°C in Cook St. The warmest $\bar{T}_{sat}$ is in Tasman Bay where mean surface temperature exceeds 15.5°C.

The ROMS mean surface temperature, $\bar{T}_{ROMS}$, shows much the same features as $\bar{T}_{sat}$, except that it is generally cooler – with the difference ranging from near zero at western end of the domain to c. −0.5°C in Tasman Bay. The overall difference over the area where MODIS and ROMS fields overlap is −0.29°C.

Monthly mean (i.e. the mean for each month of the year) values of surface temperature were computed from both satellite and ROMS data (Figures 4 and 5, respectively), and illustrate the annual cycle in temperature. In winter (June to August), surface temperature is at its coolest and shows a general northwest-to-southeast gradient with warmest values offshore to the northwest, and coldest values in Cook Strait and Tasman and Golden Bays.

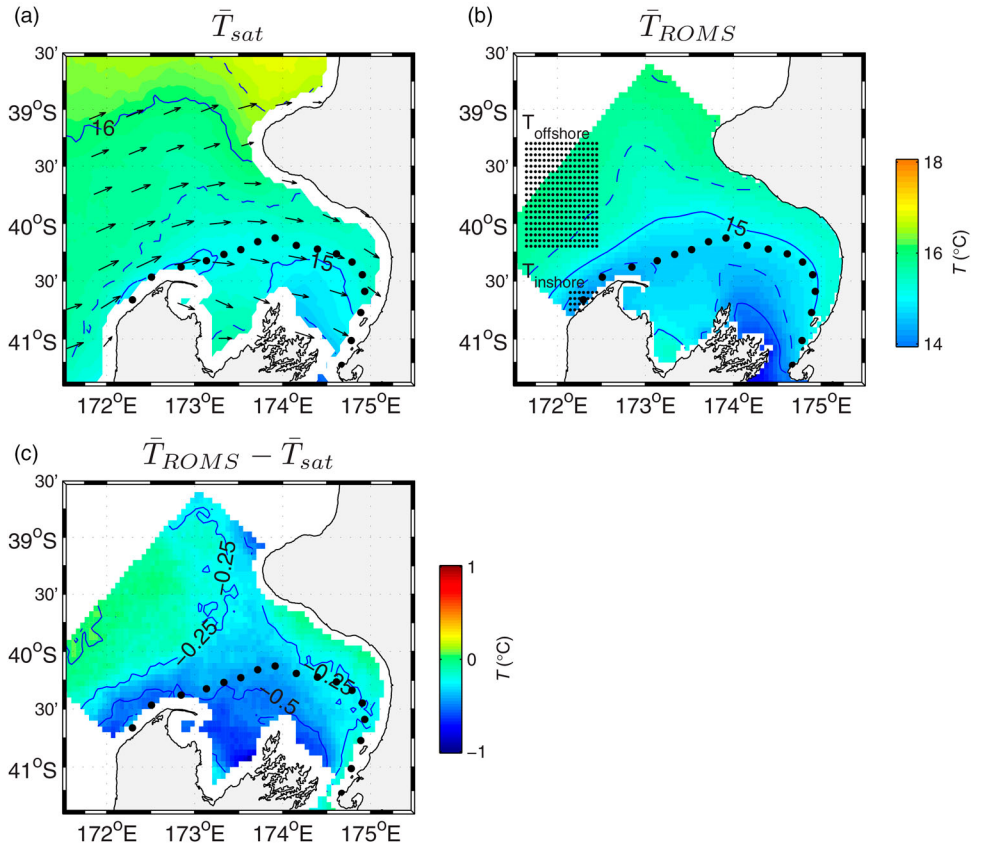

Figure 3. Mean sea surface temperature for GCS region for 2008–2013. (a) Mean surface temperature derived from MODIS satellite data, $\bar{T}_{sat}$, vectors are mean winds from the NZLAM hindcast (see text); (b) Mean surface temperature derived from ROMS simulation, $\bar{T}_{ROMS}$. Geographic locations of the sea surface temperature used to compute the upwelling index $\Gamma = T_{offshore} - T_{inshore}$ are shown as black dots; (c) Difference between ROMS and satellite estimates of mean surface temperature, $\bar{T}_{ROMS} - \bar{T}_{sat}$. The sequence of dots shows the daily locations of a numerical surface drifter released over the Kahurangi Shoals (see Figure 1).

There is no evidence of a cool plume in winter. However, starting in September, the spatial patterns in surface temperature start to change towards the summer (December to February) pattern where warmest waters are in Tasman and Golden Bay and along the east coast of the North Island. The first clear evidence of a cool plume in the monthly mean occurs in October, when surface temperature in Tasman and Golden Bays rises above 13.5°C. Surface temperature peaks in February, when it reaches 20°C along the coast of the North Island and in Tasman Bay. Surface temperature starts to cool in March, and by June has cooled enough so that any upwelling ceases to be visible.

ROMS-derived monthly means (Figure 5) tend to be smoother and cooler than the satellite-derived monthly means, but otherwise show much the same features and progression through the year. For example, both ROMS and satellite show the first appearance of the cool plume is in October, when Tasman Bay starts to get warmer than central GCS. Both ROMS and satellite show similar patterns for the excursion of cooler water into GCS from Cook St.

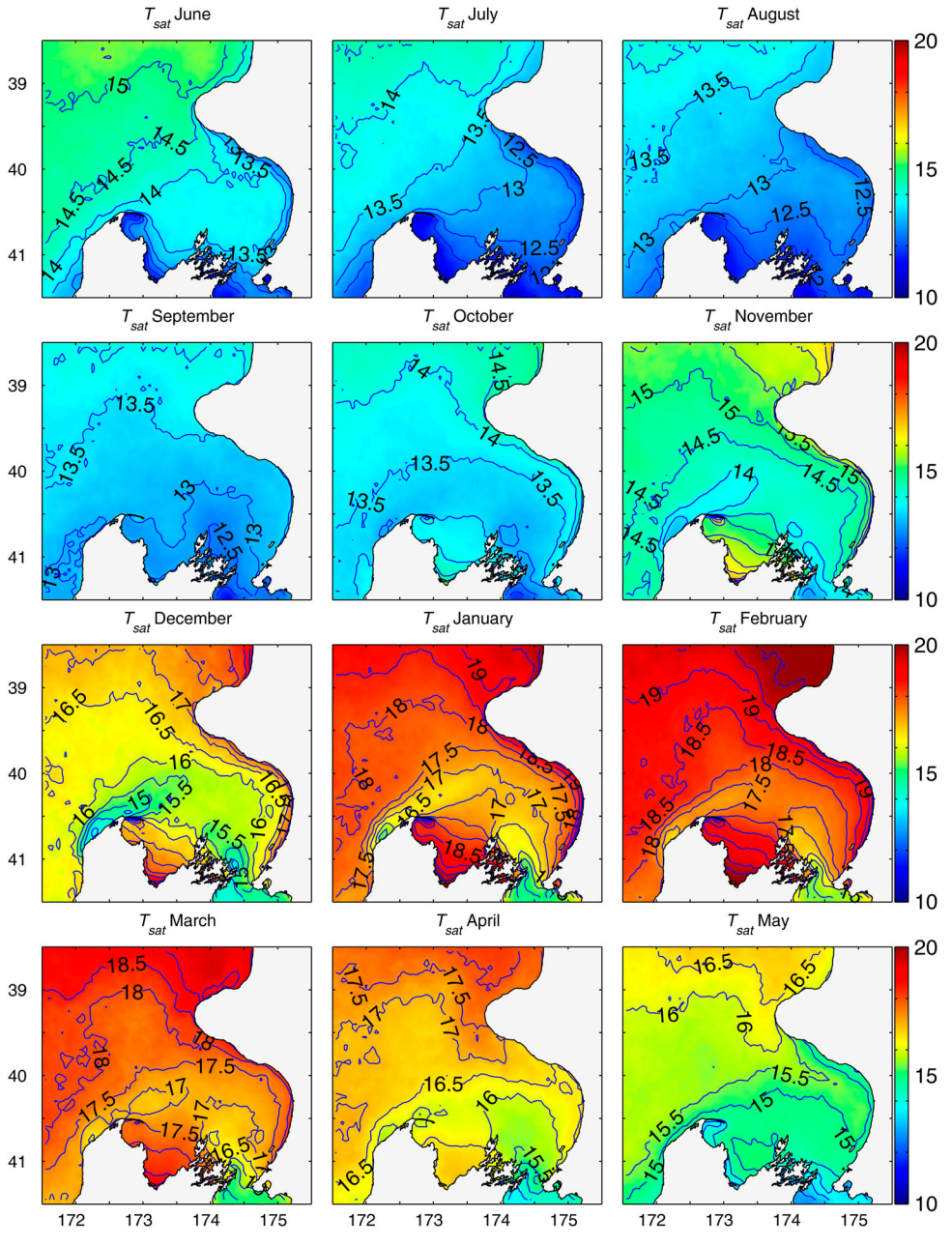

Figure 4. Monthly mean sea surface temperature for GCS derived from MODIS satellite data, T_{sat}. Each panel shows the temperature for that month averaged over the years 2008–2013.

Differences between these fields (ROMS—satellite, not shown) show that ROMS surface temperature tends to be cooler than satellite surface temperature in the central GCS, but often warmer offshore to the west, similar to the pattern shown in the mean differences (Figure 3). The difference fields do not evolve monotonically, for example, the month with the coolest differences (November, mean = −0.45°C) is followed by the

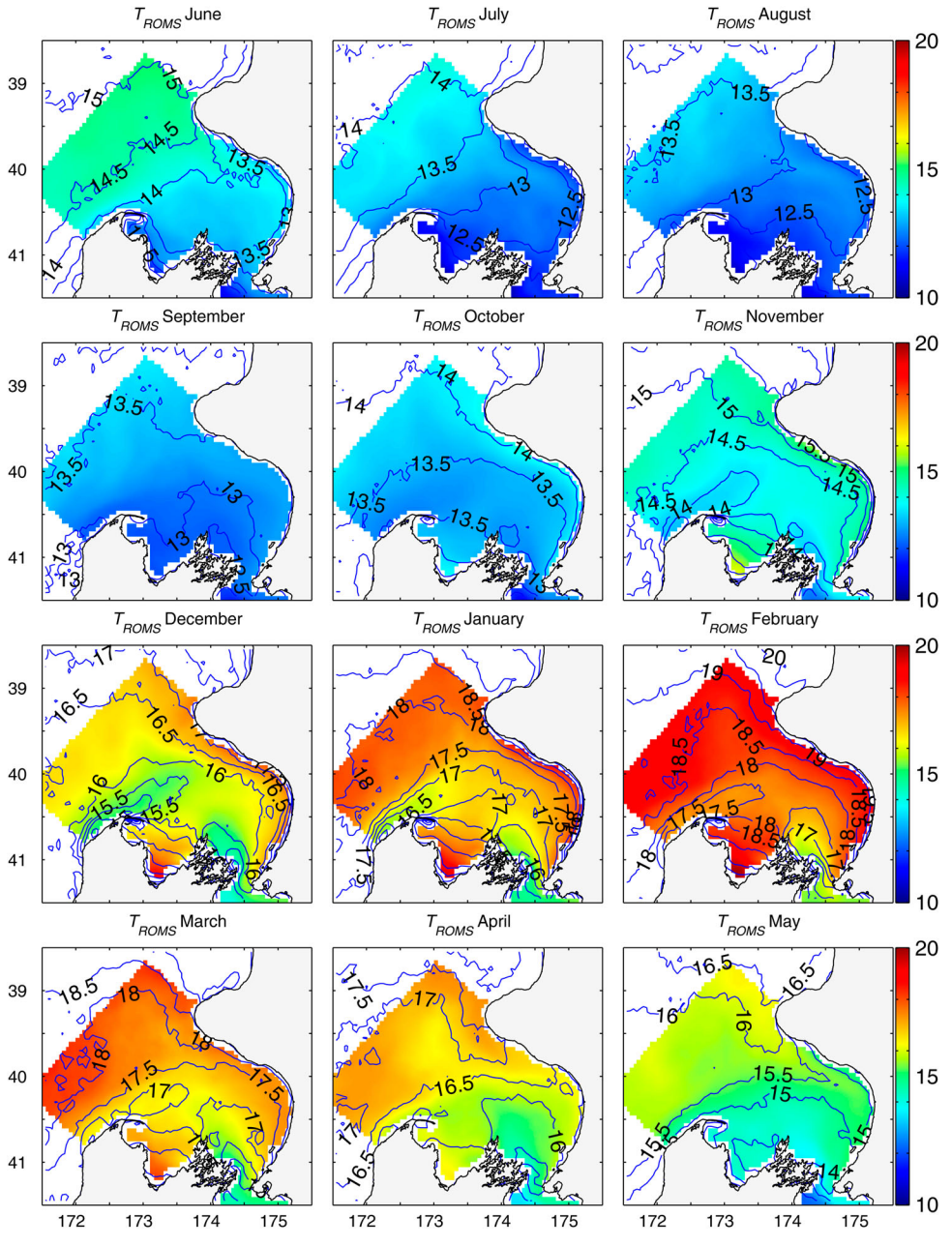

Figure 5. Monthly mean sea surface temperature for GCS derived from ROMS simulation, T_{ROMS}. Each panel shows the temperature for that month averaged over the years 2008–2013.

month with one of the warmest differences (December, mean = 0.14°C). The months with best agreement are in winter (June, mean = −0.14°C) and summer (February, mean = −0.1°C).

The annual cycles of surface temperature from both satellite and ROMS are plotted as a function of space (Figure 6) and show that almost everywhere, surface temperature

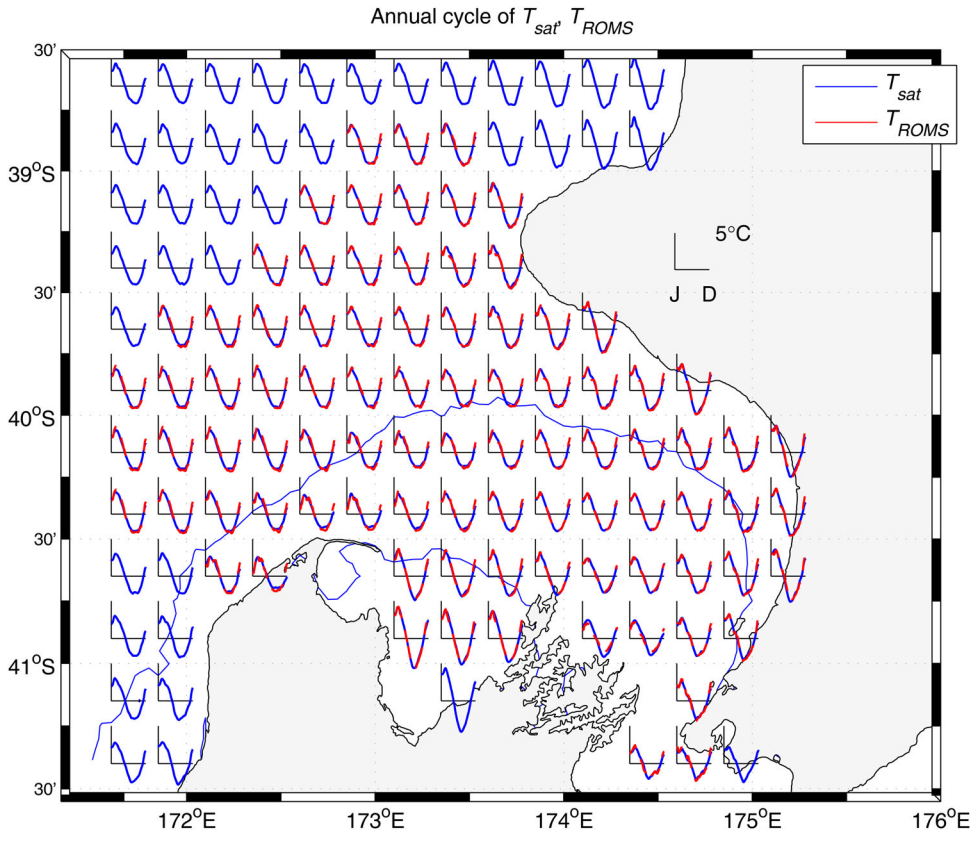

Figure 6. Annual cycles of sea surface temperature for GCS, plotted as a function of location. Each annual cycle is plotted from January to December, with the graph origin at the geographical location of the data used to compute the annual cycle. The scale is shown in the upper right hand corner. Annual cycles derived from MODIS satellite are shown in blue. Annual cycles derived from the ROMS simulation are shown in red.

has a near-sinusoid annual cycle, with minimum and maximum temperatures in August and February, respectively. The highest annual range in surface temperature of c. 9°C occurs in Tasman Bay, compared to c. 5.5°C offshore. Differences between ROMS and satellite annual cycles are relatively small. Almost everywhere ROMS annual cycles peak at the same time as the satellite cycles, but are often delayed in the minimum in winter.

Sea surface chlorophyll climatology

Mean surface chlorophyll throughout GCS ($\bar{C}_{sat}$, Figure 7) was computed over 2008 to 2013 to be consistent with the time period used for mean surface temperature. $\bar{C}_{sat}$ is generally between 0.5 and 1 mg m^{-3} with higher values along the coast and in Golden and Tasman Bays. The highest values of $\bar{C}_{sat}$ are in Golden Bay, and reach c. 2 mg m^{-3} but these are likely contaminated by suspended sediment and may not be reliable. A region of elevated $\bar{C}_{sat}$ extends north-east into GCS from near Cape Farewell with $\bar{C}_{sat}$ c. 1 to

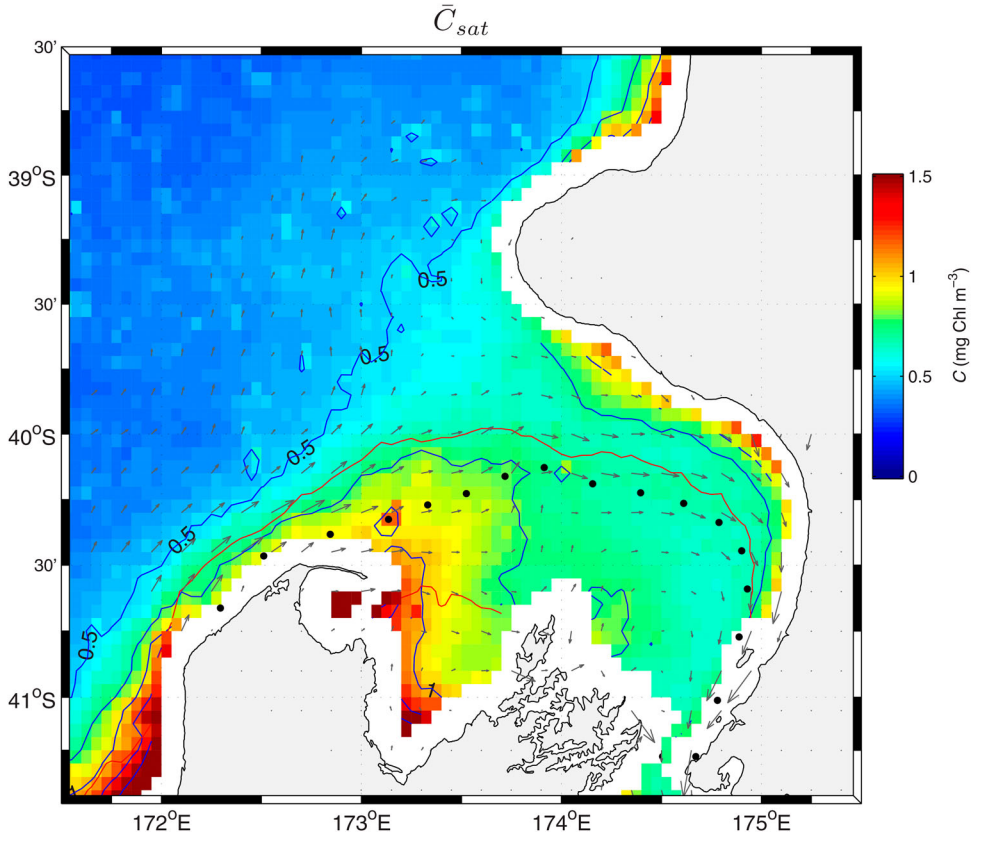

Figure 7. Mean sea surface chlorophyll-a concentration for GCS derived from MODIS satellite for the years 2008–2013. Data within 10 km of the coast are excluded to avoid sediment contamination.

0.75 mg m^{-3}. This lobe is co-located with the plume of cooler surface temperature. A second lobe of high $\bar{C}_{sat}$ is centred north of Stephens Island, and mean $\bar{C}_{sat}$ is low in Cook St.

Figure 8 shows monthly mean surface chlorophyll with monthly mean surface temperature contours overlaid. In winter (June–August), surface chlorophyll is generally less than 0.5 mg m^{-3} across the region, except close to the coast and in Tasman and Golden Bays. There is also a weak (c. 0.75 mg m^{-3}) band extending across the western GCS that appears to emanate from near Cape Farewell. In September, a spring bloom starts across the region (Chiswell et al. 2013) which continues through November, with surface chlorophyll over most of the region peaking near 0.75 mg m^{-3} in October. From June to September, there is little evidence of either a cool plume in surface temperature (Figure 4) or an associated plume in surface chlorophyll. The cool plume becomes visible in October, and initially, surface chlorophyll shows elevated levels on the southern side of the plume. However, from January to March, elevated surface chlorophyll appears to be coincident with the plume. From April onwards, the cool plume becomes weaker as the temperature heads towards winter values, although there is still a suggestion of elevated surface chlorophyll coincident with upwelled water.

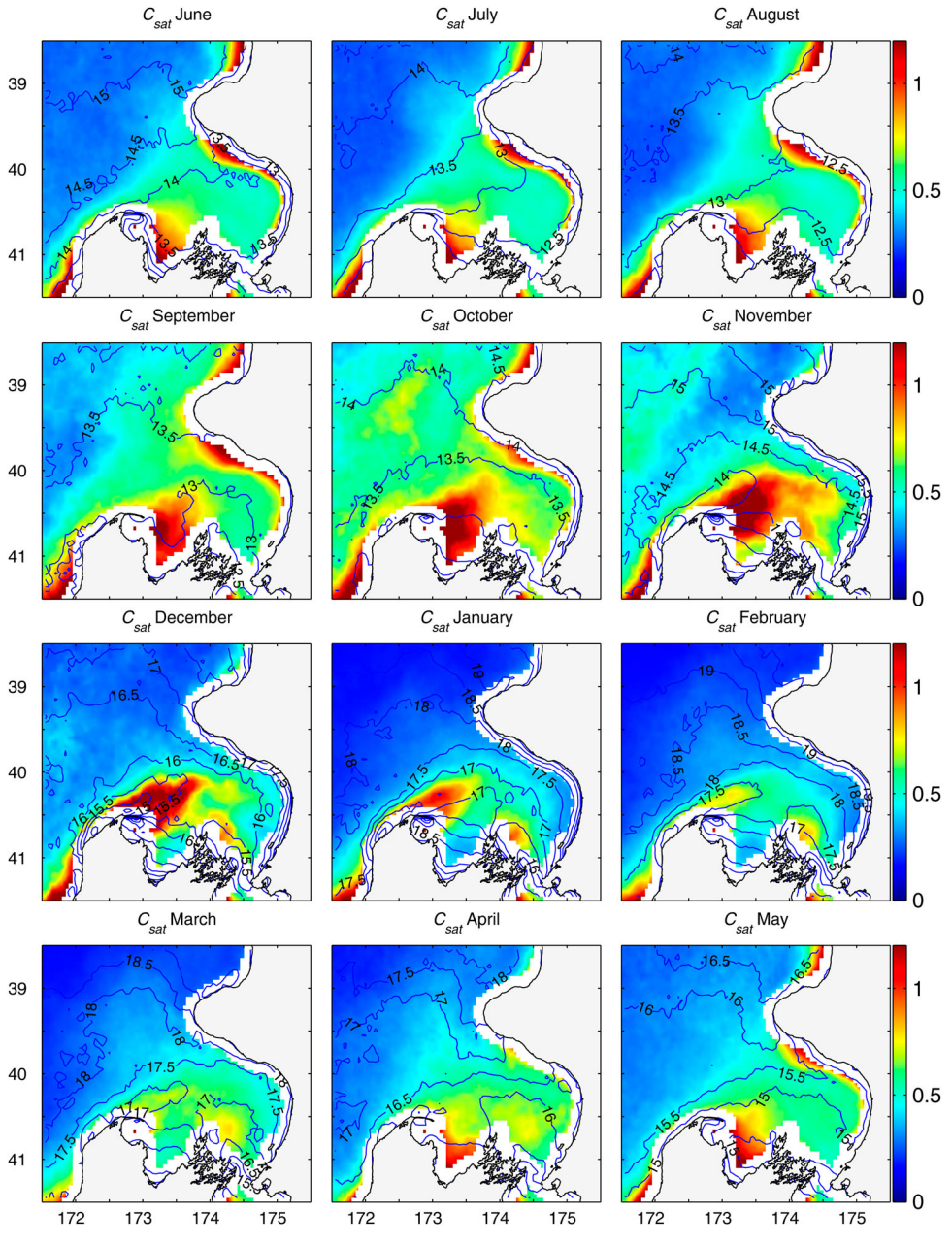

Figure 8. Monthly mean sea surface chlorophyll for GCS, derived from MODIS satellite. Each panel shows the mean surface chlorophyll for that month over the years 2008–2013. Contours of monthly mean surface temperature (see Figure 4) are superimposed as blue lines. Data within 10 km of the coast are excluded to avoid sediment contamination.

As well as elevated surface chlorophyll associated with the cool plume, there is often a second region of elevated surface chlorophyll north of Stephens Island and adjacent to Pelorus Sound entrance, which is especially visible in summer (December–March). At

times, this region is contiguous with the surface temperature plume extending through the western GCS.

Unlike annual cycles of surface temperature, annual cycles of surface chlorophyll show considerable spatial variability (Figure 9). The 15°C mean surface temperature contours have been superimposed on the figure to indicate the approximate extent of the influence of the upwelling (see Figure 3), and annual cycles of surface chlorophyll where the mean surface temperature is less than 15°C are shown in red.

Offshore in the Tasman Sea, surface chlorophyll follows the classical cycle for subtropical water and shows a small autumn bloom followed by a stronger spring bloom with minimum values in summer (Chiswell et al. 2013, 2015). Where mean temperature is less than 15°C, the influence of the upwelled water becomes apparent with the annual cycles close to Farewell Spit showing a strong early summer peak. As one progresses downstream along the mean plume, the annual cycles become flatter, so that there are regions for example in Cook St, where surface chlorophyll is essentially uniform all year round.

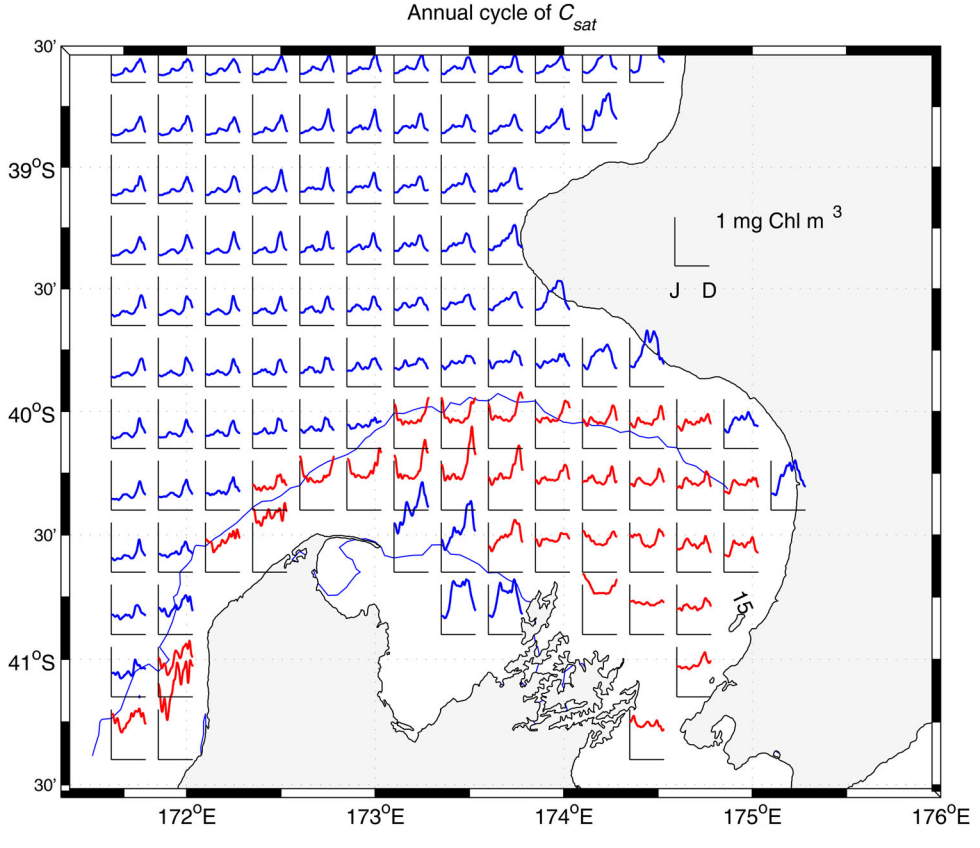

Figure 9. Annual cycles of surface chlorophyll for GCS, plotted as a function of location. Each annual cycle is plotted from January to December, with the graph origin at the geographical location of the data used to compute the annual cycle. The scale is shown in the upper right hand corner. Also shown are the 15°C isotherms of mean sea surface temperature. Annual cycles surface chlorophyll where the mean surface temperature is less than 15°C are plotted in red.

Upwelling index from surface temperature

Cool water inshore over the Kahurangi Shoals should be an indicator of upwelling, suggesting that satellite-determined surface temperature can be used to quantify upwelling. As a measure of the surface expression of upwelling, we compute an index that measures the temperature difference between inshore and offshore waters

$$\Gamma(t) = T_{\text{offshore}}(t) - T_{\text{inshore}}(t), \tag{1}$$

where T_{offshore} and T_{inshore} are the surface temperature averaged over the two regions indicated in Figure 3. The inshore area was chosen to cover the Kahurangi Shoals. The offshore area had to be large enough to average out spatial variations in surface temperature due to mesoscale eddies. Without direct observations of upwelling, testing how well Γ measures upwelling can only be done in the ROMS simulation. But before this can be done, we need to determine how well the simulation obtains this index.

Time series of T_{offshore} and T_{inshore} were computed for both satellite and simulation. The simulation values were smoothed with a 5-day window to account for the 5-day compositing of the satellite data. Inspection of these time series (Figure 10) shows that for both

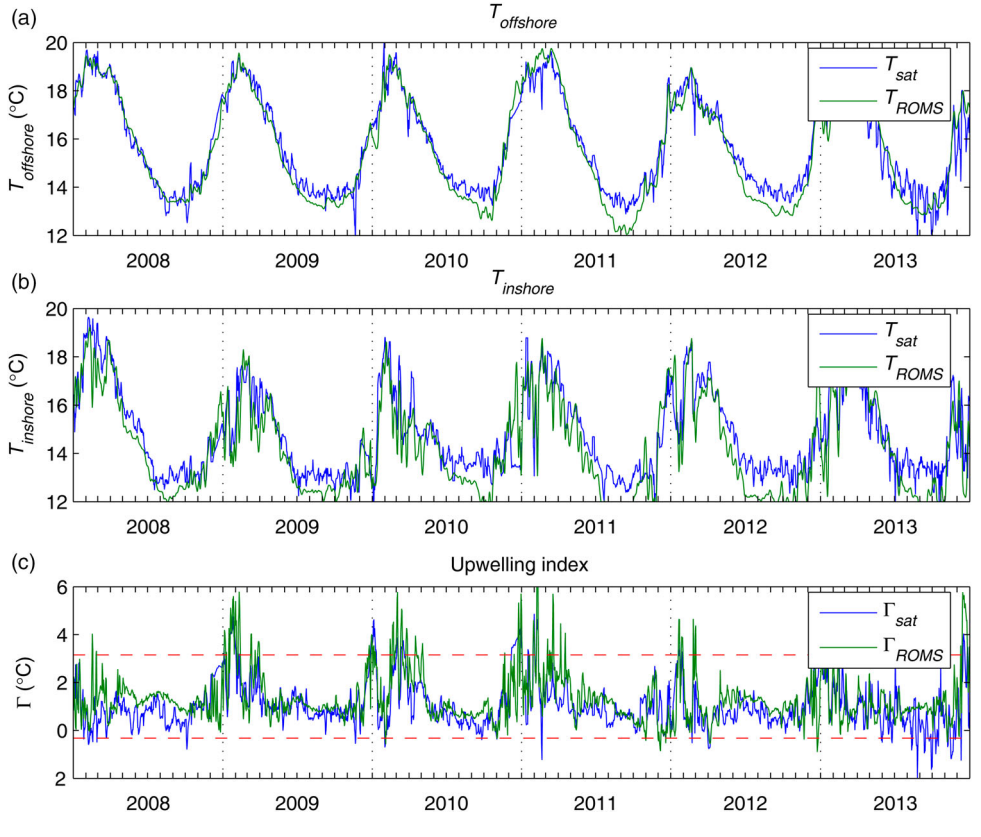

Figure 10. (a) T_{offshore}; (b) T_{inshore}; and (c) Upwelling index, $\Gamma = T_{\text{offshore}} - T_{\text{inshore}}$ (see Figure 3) plotted as a function of time for MODIS satellite-derived data (blue) and ROMS simulation (green). Horizontal lines in (c) indicate the upper and lower deciles of Γ_{sat} used to determine extreme upwelling or downwelling events (see text).

Γ_{sat} and $T_{inshore}$, the simulation tends to produce temperatures that match the data well in summer, but tend to be too cool in winter, especially at the inshore site. In summer, much of the mesoscale variability in temperature is well matched in the simulation, for example, the simulation reproduces most of the strong 2–3 week oscillations seen in $T_{inshore}$ during early 2009.

Whether derived from simulation or satellite, the upwelling index, Γ (Figure 10(c)), shows little variability during winter, but in summer, Γ shows large mesoscale fluctuations during which inshore waters can become as much as 6°C cooler than offshore. Generally, the simulation captures the timing of these fluctuations well although often the simulation amplitudes are less than the satellite amplitudes.

Both simulation and satellite Γ range from −1 to +6°, with a mean value of c. 1.0°C. Horizontal lines in Figure 10(c) indicate the upper and lower deciles of Γ, and we classify times when the index was outside of these thresholds as 'upwelling' or 'downwelling' events, even though negative Γ may not necessarily be an index of downwelling. Neutral events are defined as when Γ was within 0.25°C of its mean value.

These events are not uniformly distributed by year, or within a year (Figure 11). Both simulation and satellite distributions suggest that upwelling events were most frequent in 2010 and least frequent in 2008. Downwelling events are more frequent in ROMS than in the satellite observations, but both ROMS and satellite indicate that downwelling events occurred more often in 2011–2013 than in 2008–2009. As expected, upwelling events generally occur only in summer. Downwelling events occur throughout the year, although they also tend to be more frequent in summer.

About 140 days of upwelling or downwelling events occurred since the start of the NZLAM winds in 2007, and Figure 12 shows satellite-derived surface temperature and surface chlorophyll for averaged over all upwelling, downwelling and neutral events, respectively. The mean NZLAM wind and ROMS surface currents during these events are also shown.

The mean of the upwelling events shows a cool plume emanating from the Kahurangi Shoals (Figure 12(a)). Over the Kahurangi Shoals, the water is low in chlorophyll, but as one progresses along the plume, surface chlorophyll rises to reach a maximum value of c. 1.25 mg m^{-3} about 85 km downstream of the shoals (Figure 12(b)). The surface velocity shows a d'Urville Current that is stronger than its mean (compare with Figure 1). Surface chlorophyll is low in Tasman Bay but high in Golden Bay and there is a lobe of high surface chlorophyll north of Marlborough Sounds centred near Stephens Island. The wind shows a regional westerly flow that is topographically steered to result in strong along-shore (south-westerly) winds near the Kahurangi Shoals and north-westerly winds through Cook St.

The mean of the downwelling events (Figure 12(c,d)) shows little evidence of a cold plume. By definition, surface temperature is warmer over the Kahurangi Shoals than offshore, and surface temperature shows little quantifiable structure, except that surface waters are generally cooler in GCS than in Tasman/Golden Bays. Winds during these downwelling events are from the south, and the ROMS simulation shows a collapse of the d'Urville Current, with flow to the northwest in the central GCS. Surface chlorophyll shows enhanced levels along the mean plume core but surface chlorophyll levels are generally much lower than during upwelling events. As with upwelling events, surface chlorophyll is low in Tasman Bay, and shows high values north of Marlborough Sounds.

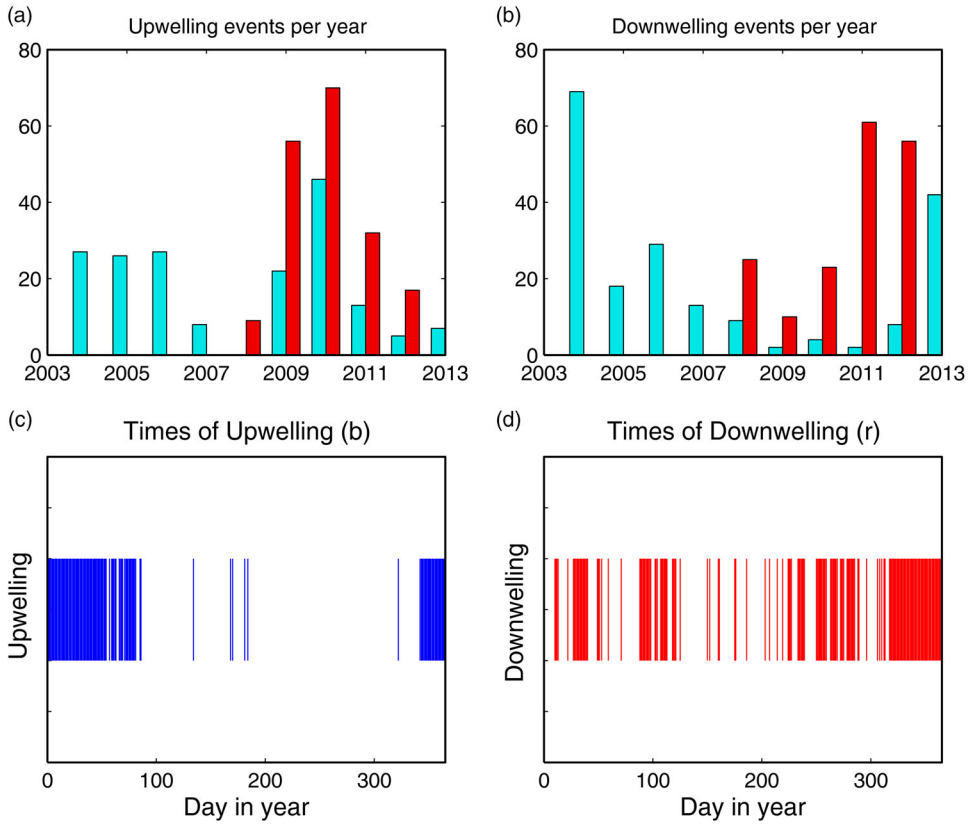

Figure 11. (a) and (b) Frequency of occurrence of extreme upwelling and downwelling events (see Figure 10) by year. Cyan shows the number of events in the MODIS satellite data, red shows the number of events in the ROMS simulation; (c) and (d) Occurrence of upwelling or downwelling events by day of the year (1 = 1 January, 365 = 31 December).

The mean of the neutral events shows surface temperature and surface chlorophyll close to their overall mean values (compare Figure 12(e) with Figure 3), with surface temperature showing a cold-core plume lying along the trajectory computed from ROMS (at least initially), and surface chlorophyll showing elevated values to the south of this core. During neutral events the wind and ocean currents are close to their mean values.

Upwelling index from ROMS simulation

The ROMS simulation can be used to test how well the temperature-based upwelling index, Γ, performs as a proxy for upwelling by computing the cross-spectrum between Γ and the vertical velocity over the Kahurangi Shoals, which we denote as w. This velocity was calculated as the average vertical velocity at the lowest level in the ROMS simulation over the inshore region shown in Figure 3.

The cross-spectrum between Γ and w was calculated using the weighted overlapped segment averaging (WOSA) method (e.g. Harris 1978). The 95% confidence limits were calculated using the method described in Thompson (1979). This cross-spectrum is

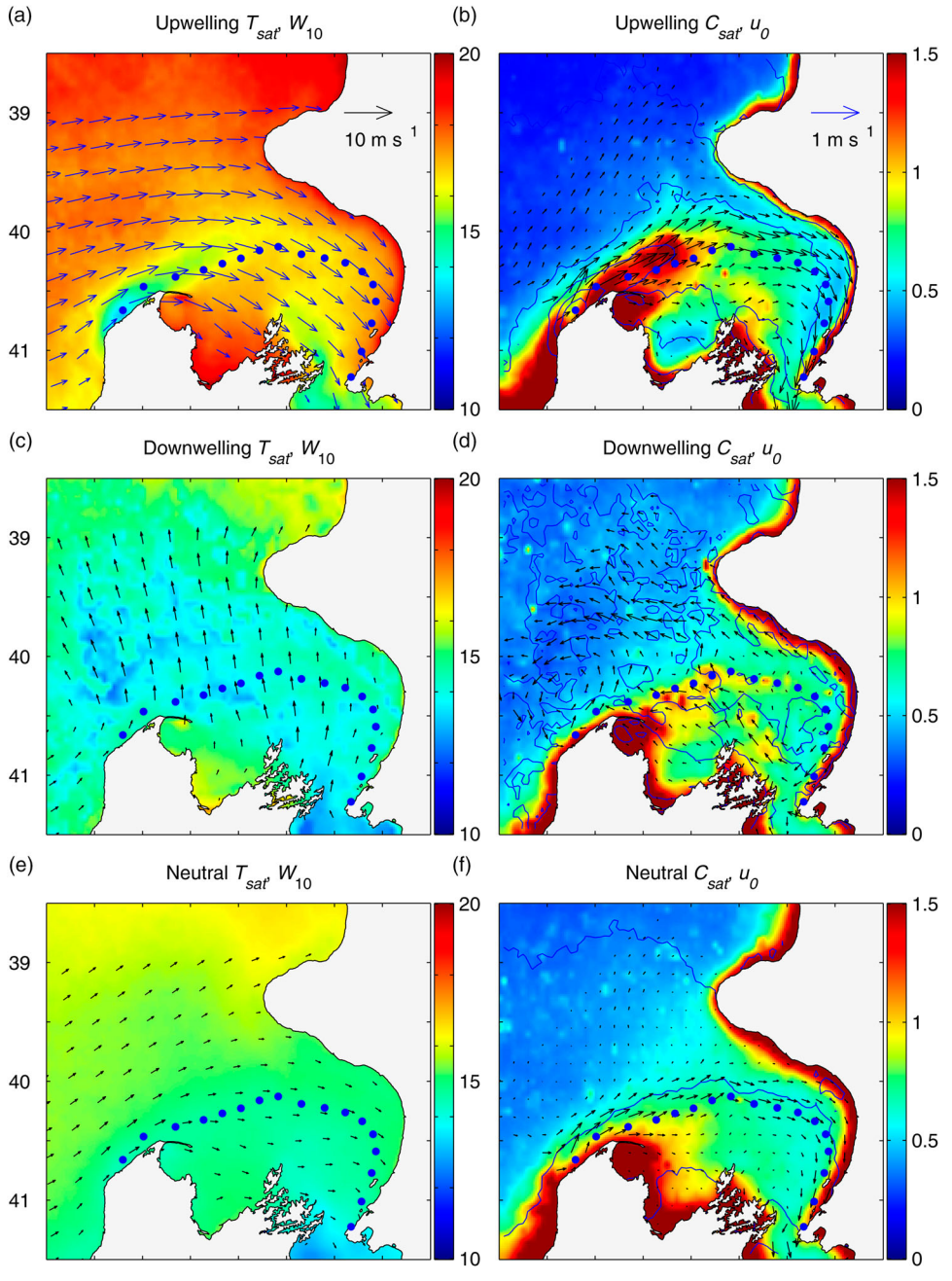

Figure 12. (a) Sea surface temperature and wind (vectors) averaged over all upwelling events (i.e. when the upwelling index exceeds the horizontal line shown in Figure 10); (b) Sea surface chlorophyll and surface velocity (vectors) averaged over all upwelling events shown in Figure 10; (c) and (d), As in (a) and (b), but for downwelling events; (e) and (f), As in (a) and (b), but for neutral events.

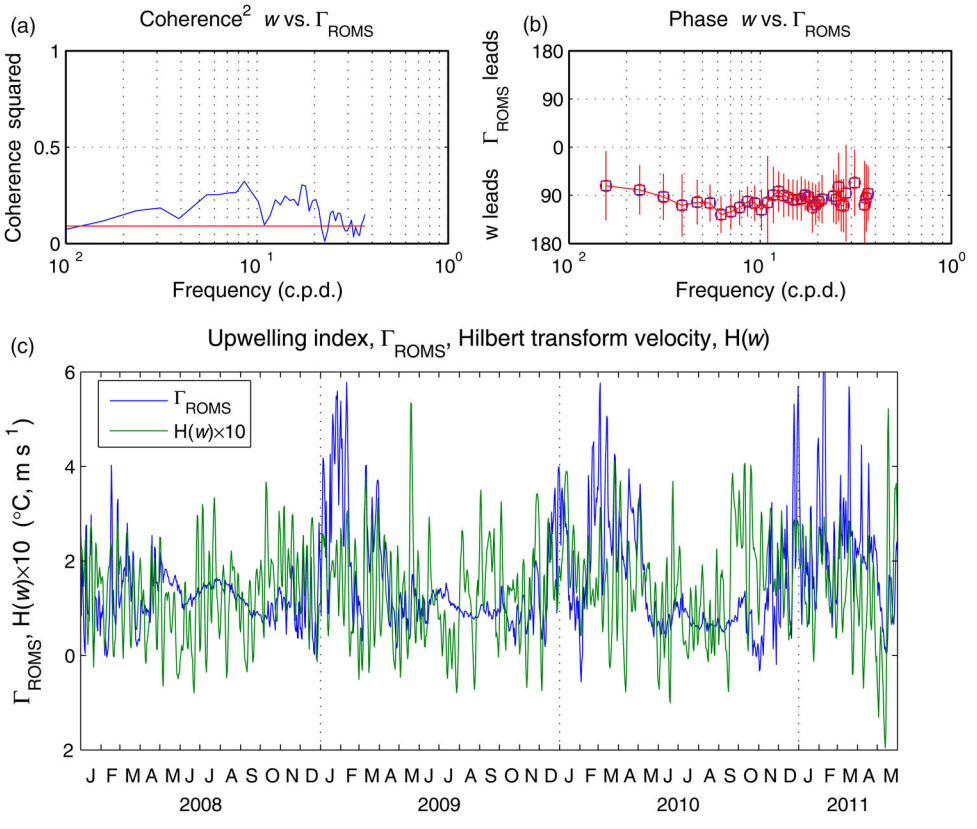

Figure 13. Comparison between upwelling index, Γ_{ROMS}, and upwelling velocity, *w*, averaged over inshore domain from ROMS sinulation (see Figure 3). (a) Coherence-squared between Γ_{ROMS} and *w*. Horizontal line shows 95% confidence limit; (b) Cross-spectral phase between Γ_{ROMS} and *w*. Phase is only shown when the coherence-squared is considered significant; (c) Time series of Γ_{ROMS} and Hilbert transform of *w*, *H*(*w*). Only 4 years are plotted for clarity. This transform preserves the spectral energy but transforms the phase by 90° (see text).

shown in Figure 13 and shows that even though coherence is low (c. 25%), it exceeds the 95% level at almost all frequencies above 10^{-2} d^{-1} (periods < 100 d). The cross-spectral phase shows that *w* leads Γ by 90° at all frequencies.

How well Γ performs as a measure of upwelling can be visualised by using a Hilbert transform to shift the phase of *w* by 90° at all frequencies, and in Figure 13(c) we show this transform, denoted as H(*w*), along with Γ. Overall, the relationship reflects the c. 25% coherence between these quantities. During winter, as expected, Γ and H(*w*) show no relationship, whereas during the summer, the fluctuations are generally in phase, although they may not have the same amplitudes.

The 90° phase shift indicates that Γ is correlated with the time-integral of *w*, $\int w dt$, which is the vertical displacement, and the cross-spectrum between Γ and this displacement is identical to that shown in Figure 13(a,b), except it shows zero phase (not shown). This suggests a simple conceptual model where the inshore temperature is determined by the vertical displacement rather than the vertical velocity.

Upwelling forcing in ROMS

The relationships between along- and cross-shore flows, upwelling and the along-shore wind can be tested in the ROMS simulation by looking at the cross-spectra between these quantities in the simulation. The along-shore direction near the Kahurangi Shoals is 41°T, and velocities from the ROMS simulation averaged over the inshore region shown in Figure 3(b) were rotated in this direction to provide the along- and cross-shore velocities, u', v'. Similarly, the NZLAM winds, W, for the grid point nearest the Kahurangi Shoals were rotated into along- and cross-shore components, then the pseudo-wind stress was calculated as $\tau_{\text{long}} = W_{\text{long}}|W|$.

Cross-spectra (Figure 14) indicate that both the along-shore and vertical velocities, u' and w, are highly coherent with the along-shore wind stress at all frequencies, having coherence-squared of about 0.4, that is, about four times the 95% confidence values. At low frequencies, both u' and w are in phase with the wind stress, but over the weather band (approximately 1–20 d periods) these components appear to lead the wind stress by 45–60°. The cross-shore velocity, v', is coherent with the wind stress at frequencies above 5×10^{-1} d^{-1} (periods < 20 d), and appears to lag the wind by 0–45°, although this phase may be statistically not different from zero.

Figure 14 suggests that the vertical velocity over the Kahurangi Shoals is highly correlated with the along-shore wind stress. A plot of the two time series (Figure 14) not only confirms this, but also indicates that upwelling occurs throughout the year. In Figure 15 we show histograms of the times when the upwelling velocity in the ROMS simulations exceeds its 90th percentile value. Thus suggests that upwelling occurrences are relatively constant from year to year, but suggests that there is an annual cycle, with upwelling occurring more often in late winter.

Summary and discussion

The presence of cool surface water plumes and increases in primary production in GCS have been known for some time. However, this work is the first that we are aware of to use both satellite observations and a numerical simulation to investigate the spatial and temporal variability in surface temperature and chlorophyll, and the relationships between the upwelling and local wind forcing.

There is little doubt that cool surface water off the Kahurangi Shoals is advected by the d'Urville Current to form cool plumes that extend into GCS. The surface temperature of the upwelled water at the Kahurangi Shoals is c. 13°C in spring and c. 17°C in late summer. As one would expect, cool plumes are only visible when the background temperature is high enough to show a surface signature and this occurs between October and April (Figure 4).

In the mean, the plume influence extends well into GCS (Figure 3). However, this influence may not always extend right up to the coast. Both the satellite data and the ROMS simulation show that in winter (June–August) there is a narrow band of cool water along the North Island west coast, conversely in summer (December–February) there is narrow band of warm water along this coast (Figure 4). Similarly, both satellite data and the simulation show that temperature south of a line running approximately between Cape Farewell and Stephens Islands shows seasonal heating and cooling and

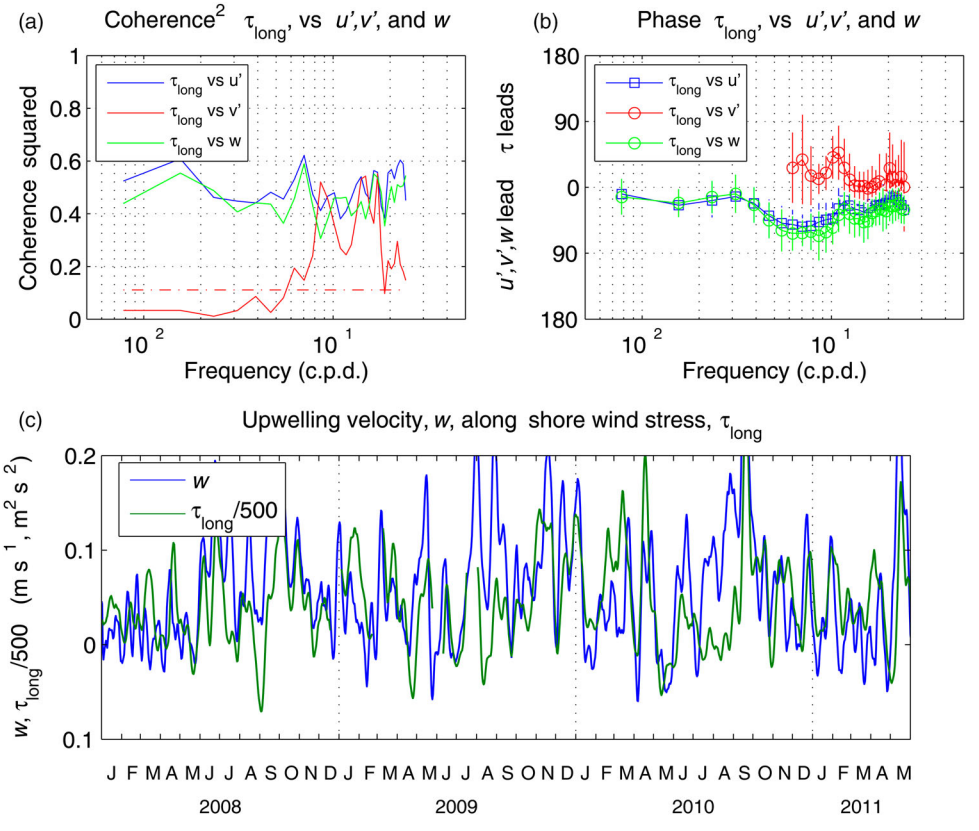

Figure 14. Cross-spectra between along-shore wind stress, τ_{long}, at the Kahurangi Shoals and the long- and cross-shore and vertical velocities, u', v', w, at the Kahurangi Shoals, from the ROMS simulation. (a) Coherence-squared. Horizontal line shows 95% confidence limit; (b). Cross-spectral phase. Phase is only shown when the coherence-squared is considered significant; (c) Along-shore (041°T) wind stress, τ_x, at the Kahurangi Shoals plotted with upwelling velocity, w, derived from ROMS simulation for the inshore region shown in Figure 3 (see text). Only 4 years are plotted for clarity.

indicates that surface temperature in Tasman and Golden Bays is little impacted by these cool plumes. To the south, surface temperature in Cook Strait is cooler than these plumes at all times of the year (Figure 4). Since mean flows in Cook Strait are likely to be to the south, this suggests that the local cooling is due to increased vertical mixing caused by strong winds and/or tides (e.g. Stevens et al. 2008; Stevens 2014).

There is also little doubt that the upwelling plumes strongly modify the primary production in GCS. In the mean (Figure 7) surface chlorophyll shows a band of higher values extending into GCS, more or less coincident with lower mean surface temperatures. Monthly satellite images show plumes of elevated surface chlorophyll extending into GCS, particularly from October to March. Early in the summer (November and December) higher surface chlorophyll is displaced to the south of the cool plume, suggesting that at times, the plumes may entrain high production stemming from waters in Golden Bay. Later (February and March) higher surface chlorophyll is spatially coincident with the cool surface temperature. In winter, the upwelling is presumably less effective in stimulating surface production, because of winter deep mixing of the water column

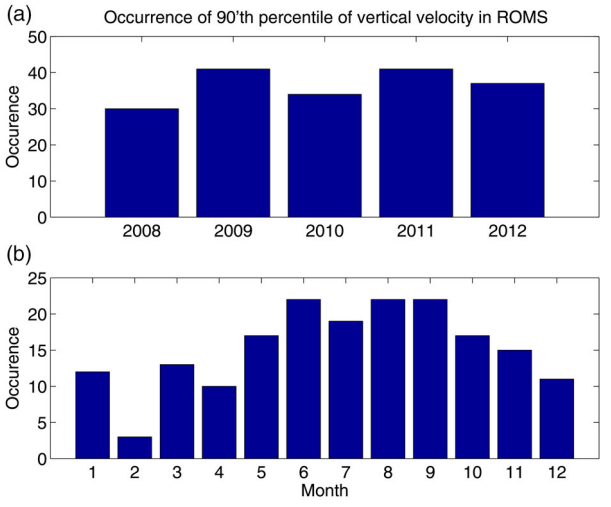

Figure 15. Histograms of times when upwelling velocity exceeds 90th percentile in ROMS simulation, (a) By year; (b) By month.

(Harris 1990) which increases light-limitation of production and homogenises the nitrate vertical distribution (Zeldis et al. 2008).

Outside of the influence of the cool plumes, annual cycles of surface chlorophyll (Figure 9) show typical autumn and spring blooms expected for subtropical waters (Chiswell et al. 2013), but within the plume influence (roughly delineated by 15°C mean surface temperature), surface chlorophyll is quite modified showing strong summer peaks. In parts of Cook St, the annual cycle is nearly flat all year round. Bradford et al. (1986) found that over much of GCS, summer time conditions in 1980 and 1981 were typical of oligotrophic waters with nitrate-nitrite levels <0.5 μ mol l^{-1}, but that upwelled water could attain levels above 4 μ mol l^{-1}.

They suggested that the injection of nutrient-rich upwelled water in summer raised surface potential primary production from <2 mg C m^{-3} h^{-1} to >5 mg C m^{-3} h^{-1}. Thus, while the injection of nutrient-rich upwelled into GCS occurs at all times of the year, it has greatest impact in summer.

Without *in situ* current measurements, it is convenient to use satellite-derived temperature difference, Γ, as an index of upwelling. The ROMS simulation demonstrates that this quantity is a reasonable index of upwelling (Figure 13), but only in summer.

The high coherence between along-shore wind and velocity components over the Kahurangi Shoals (Figure 14) suggests that the upwelling is driven by the local wind. There appears to be a change in mechanism at about 0.05 c.p.d. (20 d period). For periods longer than 20 days, the along-shore current and wind stress are effectively in phase. For shorter periods, it appears that the wind stress leads the cross-shore velocity by a few degrees and that the along-shore and vertical velocity lead the wind stress by a few degrees.

This argues for a simple Ekman mechanism where the along-shore velocity is driven by the winds, the Coriolis acceleration then sets up a cross-shore pressure gradient with lowered sea level inshore that both drives the upwelling and cross-shore velocity much as discussed by Heath and Gilmour (1987). The response of the d'Urville Current at the Kahurangi Shoals is clearly a response to GCS wide winds, rather than just the local

winds (Figure 12). Given the complicated geometry of the region, it is perhaps not surprising that the Kahurangi Shoals along-shore currents appear to lead the local wind, yet the net result is that there is a strong visual correlation between along-shore wind and vertical velocity – almost every oscillation in wind stress is matched by a corresponding oscillation in vertical velocity (Figure 14).

These findings are consistent with those of Zeldis et al. (2013) who concluded that westerly/north-westerly (i.e. along-shore) wind stress at Farewell Spit/Brothers Island was correlated with plumes of relatively cool water through the STB in summer.

Thus, in summary, this work confirms many of the previous notions of the region. We find that upwelling off the Kahurangi Shoals is strongly wind-driven in the weather band, and that upwelled water advects into GCS, where it mixes and presumably slumps. The net effect is that the surface temperature warms along the path of the plume. We find that upwelling occurs at all times of the year, but that its surface signature is only visible in summer months. The upwelled nutrient-rich water supports increased primary production compared to surrounding waters, particularly in summer when surrounding surface waters are nutrient depleted.

Further work requires more analysis of numerical simulations, with particular emphasis on both the physics and biogeochemistry. Of particular interest are questions such as – how much net primary production does the upwelling contribute to GCS including the important Pelorus Sound and Golden and Tasman Bays regions? Is the increased primary production limited by the increased nutrient supply or are there are other limiting factors, such as residence time in GCS? Is nutrient loading at Pelorus Sound entrance a manifestation of the Kahurangi Shoals upwelling, or is it related to separate upwelling adjacent to the Marlborough Sounds under westerly/north-westerly conditions? A biogeochemical model added to the hydrodynamic simulations will allow us to further understand the temporal and spatial (horizontal and vertical) distributions of nutrient and production dynamics of the GCS region to address these questions.

Acknowledgements

We thank Craig Stewart for processing Golden Bay mooring data, Simon Wood for MODIS data processing and Trevor Cary-Smith for NZLAM data. We acknowledge the contribution of New Zealand eScience Infrastructure (NeSI) to the ROMS modelling used in this research. New Zealand's national computer and analytics services are funded jointly by NeSI's collaborator institutions and through the Ministry of Business, Innovation and Employment (http://www.nesi.org.nz). We thank two anonymous reviewers for their efforts in reviewing this article. Associate editor: Associate Professor Craig Stevens.

Disclosure statement

No potential conflict of interest was reported by the authors.

Funding

This work was funded by the Ministry of Business, Innovation and Employment (MBIE), New Zealand through grants to NIWA, via the Aquaculture/Environment Interactions and Ecosystem Structure and Function programmes [grant numbers ACEE 1703 and COES 1601]. MODIS data were used courtesy of NASA Goddard Space Flight Center.

References

Bowman MJ, Lapennas PP, Murtagh R, Chiswell SM, Foster B, Battaerd W, Wilkinson V. 1983. Coastal upwelling, cyclogenesis and squid fishing near Cape Farewell, New Zealand. In: Gade H, editor. Coastal oceanography. New York: Plenum; p. 279–310.

Bradford JM, Chapman B. 1988. *Nyctiphanes australis* (Euphausiacea) and an upwelling plume in western Cook Strait, New Zealand. New Zealand Journal of Marine and Freshwater Research. 22 (2):237–247.

Bradford JM, Lapennas PP, Murtagh RA, Chang FH, Wilkinson V. 1986. Factors controlling summer phytoplankton production in greater Cook Strait, New Zealand. New Zealand Journal of Marine and Freshwater Research. 20(2):253–279.

Bricaud A, Roesler C, Zaneveld JRV. 1995. In situ methods for measuring the inherent optical properties of ocean waters. Limnology and Oceanography. 40(2):393–410.

Chiswell SM, Bradford-Grieve J, Hadfield MG, Kennan SC. 2013. Climatology of surface chlorophylla, autumn-winter and spring blooms in the southwest Pacific Ocean. Journal of Geophysical Research: Oceans. 118(2):1003–1018.

Chiswell SM, Calil PHR, Boyd PW. 2015. Spring blooms and annual cycles of phytoplankton: a unified perspective. Journal of Plankton Research. 37(3):500–508.

Esaias WE, Abbott MR, Barton I, Brown OB, Campbell JW, Carder KL, Clark DK, Evans RH, Hoge FE, Gordon HR, et al. 1998. An overview of MODIS capabilities for ocean science observations. IEEE Transactions on Geoscience and Remote Sensing. 36(4):1250–1265.

Foster BA, Battaerd WR. 1985. Distribution of zooplankton in a coastal upwelling in New-Zealand. New Zealand Journal of Marine and Freshwater Research. 19(2):213–226.

Garner DM. 1954. Sea surface temperature in the South-West Pacific Ocean, from 1949 to 1952. New Zealand Journal of Science and Technology. B, General Section. 36(3):285–303.

Harris FJ. 1978. On the use of windows for harmonic analysis with the discrete Fourier transform. Proceedings of the IEEE. 66(1):51–83.

Harris TFW. 1990. Greater Cook Strait: form and flow. Wellington: DSIR Marine and Freshwater. 212 pp.

Heath RA, Gilmour AE. 1987. Flow and hydrological variability in the Kahurangi plume off northwest South Island, New Zealand. New Zealand Journal of Marine and Freshwater Research. 21 (1):125–139.

Kalnay E, Kanamitsu M, Kistler R, Collins W, Deaven D, Gandin L, Iredell M, Saha S, White G, Woollen J, et al. 1996. The NCEP/NCAR 40-year reanalysis project. Bulletin of the American Meteorological Society. 77(3):437–471.

Lee ZP, Carder KL, Arnone RA. 2002. Deriving inherent optical properties from water color: a multiband quasi-analytical algorithm for optically deep waters. Applied Optics. 41(27):5755–5772.

Lee ZP, Lubac B, Werdell J, Arnone RA. 2009. An update of the quasi-analytical algorithm (QAA_v5). International Ocean Color Group Software Report, 1–9. Available from: www.ioccg.org/groups/Software_OCA/QAA_v5.pdf

Lorenc AC, Ballard SP, Bell RS, Ingleby NB, Andrews PLF, Barker DM, Bray JR, Clayton AM, Dalby T, Li D, et al. 2000. The met. Office global three-dimensional variational data assimilation scheme. Quarterly Journal of the Royal Meteorological Society. 126(570):2991–3012.

Marchesiello P, McWilliams JC, Shchepetkin A. 2001. Open boundary conditions for long-term integration of regional oceanic models. Ocean Modelling. 3(1–2):1–20.

Reynolds RW, Smith TM, Liu C, Chelton DB, Casey KS, Schlax MG. 2007. Daily high-resolution-blended analyses for sea surface temperature. Journal of Climate. 20(22):5473–5496.

Shirtcliffe TGL, Moore MI, Cole AG, Viner AB, Baldwin R, Chapman B. 1990. Dynamics of the cape farewell upwelling plume, New Zealand. New Zealand Journal of Marine and Freshwater Research. 24(4):555–568.

Smith SD. 1988. Coefficients for sea surface wind stress, heat flux, and wind profiles as a function of wind speed and temperature. Journal of Geophysical Research: Oceans. 93(C12):15467–15472.

Stanton BR. 1971. Hydrology of Karamea bight, New Zealand. New Zealand Journal of Marine and Freshwater Research. 5(1):141–163.

Stevens C. 2014. Residual flows in Cook Strait, a large tidally dominated strait. Journal of Physical Oceanography. 44(6):1654–1670.
Stevens C, Sutton P, Smith M, Dickson R. 2008. Tidal flows in Te Aumiti (French Pass), South Island, New Zealand. New Zealand Journal of Marine and Freshwater Research. 42(4):451–464.
Thompson RORY. 1979. Coherence significance levels. Journal of the Atmospheric Sciences. 36 (10):2020–2021.
Torres LG. 2013. Evidence for an unrecognised blue whale foraging ground in New Zealand. New Zealand Journal of Marine and Freshwater Research. 47(2):235–248.
Walters DN, Williams KD, Boutle IA, Bushell AC, Edwards JM, Field PR, Lock AP, Morcrette CJ, Stratton RA, Wilkinson JM, et al. 2014. The met office unified model global atmosphere 4.0 and JULES global land 4.0 configurations. Geoscientific Model Development. 7(1):361–386.
Walton CC, Pichel WG, Sapper JF, May DA. 1998. The development and operational application of nonlinear algorithms for the measurement of sea surface temperatures with the NOAA polar-orbiting environmental satellites. Journal of Geophysical Research: Oceans. 103(C12):27999–28012.
Wang M, Shi W. 2007. The NIR-SWIR combined atmospheric correction approach for MODIS ocean color data processing. Optics Express. 15(24):15722–15733.
Wilkin JL, Arango HG, Haidvogel DB, Lichtenwalner CS, Glenn SM, Hedström KS. 2005. A regional ocean modeling system for the long-term ecosystem observatory. Journal of Geophysical Research: Oceans. 110(C6). doi:10.1029/2003JC002218
Zeldis JR, Hadfield MG, Booker DJ. 2013. Influence of climate on Pelorus sound mussel aquaculture yields: predictive models and underlying mechanisms. Aquaculture Environment Interactions. 4 (1):1–15.
Zeldis JR, Howard-Williams C, Carter CM, Schiel DR. 2008. ENSO and riverine control of nutrient loading, phytoplankton biomass and mussel aquaculture yield in Pelorus Sound, New Zealand. Marine Ecology Progress Series. 371:131–142.